NASA Contractor Report 175049

Fatigue Crack Growth Under General-Yielding Cyclic-Loading

Zheng Minzhong and H.W. Liu
Syracuse University
Syracuse, New York

February 1986

Prepared for
Lewis Research Center
Under Grant NAG 3-348

NASA
National Aeronautics and
Space Administration

FOREWORD

The work was conducted at the George Sachs Fracture and Fatigue Research Laboratory at Syracuse University. The financial support provided by NASA, Grant No. NAG 3-348, and a Visiting Scholarship from the People's Republic of China for Mr. Zheng Minzhong are acknowledged. The authors wish to thank the Academic Computing Center of Syracuse University for making computer time available and Hibbitt, Karlsson, and Sorensen, Inc., for the privilege of using the ABAQUS finite-element program.

FATIGUE CRACK GROWTH UNDER GENERAL-YIELDING CYCLIC-LOADING

Zheng Minzhong,* Visiting Scholar

and

H. W. Liu, Professor of Mechanical and Aerospace Engineering

Syracuse University

Syracuse, New York 13210

SUMMARY

In low cycle fatigue, cracks are initiated and propagated under general-yielding cyclic-loading. For general-yielding cyclic-loading, Dowling and Begley have shown that fatigue crack growth rate correlates well with the measured ΔJ. The correlation of da/dN with ΔJ has also been studied by a number of other investigators. However, none of these studies has correlated da/dN with ΔJ calculated specifically for the test specimens.

Solomon measured fatigue crack growth in specimens in general-yielding cyclic-loading. The crack tip fields for Solomon's specimens are calculated using the finite element method and the J-values of Solomon's tests are evaluated. The measured crack growth rate in Solomon's specimens correlates very well with the calculated ΔJ.

INTRODUCTION

In strain-controlled fatigue or low cycle fatigue, cracks are initiated and propagated under general-yielding cyclic-loading. There-

---

*Aircraft Strength Research Institute
Xian, People's Republic of China.

fore, linear elastic fracture mechanics can no longer be used to analyze fatigue crack growth rate.

Dowling and Begley [1] and Dowling [2] correlated fatigue crack growth rate with ΔJ as shown in Figure 1. The value of J was evaluated as the rate of change of the deformation work density with respect to crack extension for through-cracks in plates. The data points in the figure were measured with specimens under general-yielding cyclic-loading, and the scatter band was obtained with the linear elastic fracture mechanics specimens. They agree very well with each other. Dowling [2] has developed an equation for calculating ΔJ for surface cracks by combining the finite element method calculations of Shih and Hutchinson [3] for center-cracked and edge-cracked panels. Haddad and Mukherjee [4] and Tanaka, Hoshide, and Nakata [5] followed the same procedure to evaluate J and correlated J with da/dN. Kaisand and Mowbray [6] correlated fatigue crack growth in general yielding with ΔJ. They divided ΔJ into two parts: elastic and plastic.

$$\Delta J = \Delta J_e + \Delta J_p \tag{1}$$

Using Shih and Hutchinson's calculation and following a procedure similar to Dowling's, ΔJ_p for a surface crack is approximated by

$$\Delta J_p = 1.96 \sqrt{1/n'}\, \Delta W_p a \tag{2}$$

where n' = the cyclic strain hardening exponent and ΔW_p = the applied plastic deformation work density.

Tomkins [7] and Tomkins, Sumner, and Wareing [8] correlated crack growth rate with crack tip opening displacement, CTOD, and J. Here, J consists of two parts

$$J = \frac{\pi\sigma^2 a}{E} + \frac{\alpha\pi\sigma\varepsilon_p a}{1+n} \qquad (3)$$

where n is the monotonic strain hardening exponent. However, in all of the above investigations (1, 2, 4, 5, 6, 7 and 8), no attempt was made to correlate da/dN data with J calculated for the specific test specimens.

Solomon [9] measured fatigue crack growth in specimens in general-yielding cyclic-loading. In this paper, the crack tip field of Solomon's specimens will be calculated with FEM. The J values will be evaluated, and the measured crack growth rate will be correlated with the calculated J values.

ANALYSIS OF SOLOMON'S EXPERIMENT

Solomon measured fatigue crack growth in 1018 steel under general-yielding cyclic-loading. The chemical composition of the steel is given in Table 1. The test section of the cylindrical specimen was reduced by two semi-curcular notches (Figure 2a). The gross cross-sectional area of the test section of the specimens was 1.24 x 12.6 mm^2. A sharp notch was used to initiate the fatigue crack. Both ends of a specimen were rigidly attached to the loading frame of the test machine. The fatigue crack growth rates were measured at six different applied cyclic plastic strain ranges. The applied strain range was controlled by the extenso-meter located 7.62 mm from the edge of the specimen as shown in Figure 2a. The total applied strain range consists of two parts

$$\Delta\varepsilon = \Delta\varepsilon_e + \Delta\varepsilon_p \qquad (4)$$

and

$$\Delta\varepsilon_e = \frac{\Delta\sigma}{E} \qquad (5)$$

Solomon [9] plotted his crack growth data in terms of pseudo stress-intensity factor defined as

$$\Delta(PK) = E(\Delta\varepsilon)\sqrt{a} \tag{6}$$

Subsequently, the data were analyzed by Haigh and Skelton [10] in terms of a strain-intensity factor defined as

$$\Delta K_{\varepsilon} = (\frac{1}{2}\Delta\varepsilon_e + \Delta\varepsilon_p)\sqrt{\pi a} \tag{7}$$

For comparison with (7), (6) can be written in the form

$$\frac{\sqrt{\pi}\,\Delta(PK)}{E} = (\Delta\varepsilon_e + \Delta\varepsilon_p)\sqrt{\pi a} \tag{8}$$

Solomon correlated his data with the total strain range $\Delta\varepsilon$. In Haigh and Skelton's analysis, the elastic strain amplitude was used instead of the elastic strain range because of the consideration of crack closure when the applied stress became compression. The data and the correlations proposed by Solomon [9] and Haigh and Skelton [10] are shown in Figure 3. The scatter band of solomon's correlation is a factor of slightly more than 3, and the scatter band is reduced to a factor of 2.5 by the Haigh and Skelton correlation.

Brown, et al. [11] calculated the plane stress crack tip field of Solomon's specimen with FEM. In their calculation, a constant stress boundary condition was used. The crack growth rate was correlated with the size of the severe strain zone, r_s. The constant stress boundary condition will introduce a bending moment at the test section, and the bending moment could be more than that experienced by the specimen.

Solomon's specimens were tested in the strain controlled fatigue test fixture. Both ends of the specimen were firmly attached to a rigid test

frame. Therefore, the test condition can best be simulated by a constant-displacement boundary condition, which was used in the present FEM calculation.

For a specimen under a general-yielding cyclic-load, the entire test section of the specimen experiences cyclic plastic deformation. The applied cyclic stress and cyclic strain as well as the crack tip cyclic stress and strain fields are related to each other through the cyclic stress-strain curve.

The cyclic yield stress ($\Delta\sigma_Y/2$ = 170 MPa) was obtained as the intersection of two straight line segments in the log $\Delta\sigma/2$ versus log $\Delta\varepsilon/2$ plot, one in the elastic region and one in the plastic region (Figure 2b). The cyclic-stress cyclic-plastic-strain relation derived from the data in Figure 2b is

$$\frac{\Delta\sigma}{2}\ (\text{MPa}) = 1360\ \left(\frac{\Delta\varepsilon_p}{2}\right)^{0.26} \tag{9}$$

where $\Delta\sigma/2$ and $\Delta\varepsilon_p/2$ are cyclic stress amplitude and cyclic plastic strain amplitude, respectively.

The complete cyclic stress-strain history experienced by the material in a crack tip region is rather complicated. As a crack tip advances ahead toward a point, the material at the point experiences increasing stress and strain ranges. As the cyclic loading goes on, the material at the point either cyclically hardens or softens. The detailed cyclic constitutive relation of the steel is unknown. Crack closure even complicates the matter further. In view of the complications of the crack tip field, it is necessary to make a few simplifying assumptions in order to calculate crack tip field for fatigue crack growth analysis.

During the loading half cycle, the material near the crack tip in the plane stress region near the specimen surface will be stretched. Upon unloading, the crack front in the plane stress region will close. Crack closure will reduce the effective stress intensity range. It is well known that the compressive residual stress and crack closure due to a tensile overload will cause crack growth retardation. Normally fatigue crack growth is measured under a tension-tension load. If a tensile overload is followed by a compressive overload, the crack retardation is greatly reduced because the crack tip compressive residual stress field and crack closure are washed out by the compressive overload [13]. For the completely reversed loading of low cycle fatigue, the large compressive strain will "flatten" the crack surface and will even up the residual stresses throughout the specimen. Therefore it is reasonable to assume that at the beginning of the tensile half cycle, the specimen is stress free, the crack tip will open as the applied stress becomes tensile as suggested by Haigh and Skelton [10], and the fatigue crack growth mechanism will become operational.

We also assume that the material at a crack tip experiences "stabilized" hysteresis loop. This assumption is reasonable if crack growth rate is slow enough and the material has experienced enough number of high strain cycles. In the small scale yielding case, the material will have to experience several thousand fatigue cycles in the monotonic plastic zone and, in addition, it will have to experience several thousand cycles of cyclic plastic deformation before it reaches the crack tip. Therefore, the hysteresis loop of the material close to the crack tip is fully stabilized. In the case of low cycle fatigue, the number of fatigue cycles is much less, but the cyclic strain range is much higher. Because of the

high strain range, it is also reasonable to expect stabilized hysteresis loop. If hysteresis loops are stabilized, the cyclic stress-strain relation can be used for the finite element calculation. One will be able to calculate the cyclic stress and cyclic strain fields by making a static calculation using the cyclic stress-strain relation, if the hysteresis loop is stabilized everywhere, and if the residual stress is negligible at the beginning of the tensile half cycle.

For Solomon's specimens, the size of the plastic zone is much larger than the plate thickness, therefore, plane stress finite element should be used. The mesh is shown in Figure 4a. The lateral curvature of the specimen was simulated by layers of different thicknesses, as illustrated in Figure 4b. The detailed mesh near the crack tip is in Figure 4c. The solid lines in 4c delineate the meshes, and the dashed curves are the paths for J-integral evaluation. All the elements in the layer closest to the crack line are of the same thickness, and the values of J-integral are evaluated along the paths within this layer.

The ABAQUS FEM program was used. The plane eight noded quadrilateral quadratic isoparametric element was used. The crack tip triangular elements were formed by collapsing one side of the quadrilateral element.

According to Hutchinson [14], and Rice and Rosengren [15], the crack tip stress and strain fields for non-linear elastic solids obeying the power-law stress-strain relation, $(\sigma/\sigma_o) = \alpha(\varepsilon/\varepsilon_o)^n$, are

$$\frac{\sigma_{ij}}{\sigma_o} = \left[\frac{1}{\alpha\varepsilon_o I_n \{r/(J/\sigma_o)\}}\right]^{\frac{n}{1+n}} \tilde{\sigma}_{ij}(\theta,n) \tag{10a}$$

$$\frac{\varepsilon_{ij}}{\varepsilon_o} = \alpha\left[\frac{1}{\alpha\varepsilon_o I_n \{r/(J/\sigma_o)\}}\right]^{\frac{1}{1+n}} \tilde{\varepsilon}_{ij}(\theta,n) \tag{10b}$$

According to Equation 10, J is capable of characterizing the entire crack tip stress and strain fields. However, the recent plane-strain finite element calculations (16, 17, 18) indicate that crack tip field characteristics are strongly dependent on specimen geometry as well as load level. In other words, at the same J-value, the crack tip field may vary widely from one specimen geometry to another. For the same specimen shape, at the same J-value, the crack tip field in a small specimen in deep general-yielding may differ considerably from that of a large specimen at a limited amount of plastic deformation. According to Equation 10, if J is capable of characterizing crack tip field, the plot of (σ_{ij}/σ_o) or $(\varepsilon_{ij}/\varepsilon_o)$ versus $r/(J/\sigma_o)$ should fall on the same curve regardless of the spceimen geometry and load level.

Crack tip stresses and strains for three crack lengths, a = 1.27, 2.54 and 5.08 mm, were calculated. The data on effective stress, (σ_e/σ_Y) and effective plastic strain $(\varepsilon_e^p/\varepsilon_Y)$ for a = 1.27 mm at various load levels are plotted against $r/(J/\sigma_Y)$ in Figure 5a. All the data in the crack tip region fall on the same curve. The slopes of the lines close to the crack tip are 0.85 and 0.23 which are slightly higher than the values given by Hutchinson [13] and Rice and Rosengren [14]; $1/(1 + n') = 0.8$ and $n'/(1 + n') = 0.2$ respectively. n' is the cyclic strain hardening exponent. Similar plots for σ_{yy} and ε_{yy} are shown in Figure 5b. Figure 6 shows the normalized strain distribution, $(\varepsilon_{yy}/\varepsilon_Y)$ versus $r/(J/\sigma_Y)$, near the crack tip for three different crack lengths. In the crack tip region, the data for all three crack lengths fall on the same straight line as suggested by Equation (10). The data in figures 5a, 5b and 6 indicate that J-integral is capable of characterizing the crack tip field. In other words, at

the same J-value, the crack tip stress and strain fields are the same regardless of the length of the crack. Since crack growth rate is controlled by crack tip field, J will be able to correlate well with Solomon's crack growth data.

Solomon's crack growth data are shown in Figure 3. At each of the data points, one can obtain the values of da/dN, $\Delta\varepsilon_p$ and crack length, a. $\Delta K_\varepsilon = \{(\Delta\varepsilon_e/2) + \Delta\varepsilon_p\} \sqrt{\pi a}$. With $\Delta\varepsilon_e$ and $\Delta\varepsilon_p$ known, the value of the crack length can be found. With both crack length and the plastic strain at x = 7.62 mm given, the value of J can be calculated. The results of the calculations for three different crack lengths, a = 1.27, 2.54, and 5.08 mm, are shown in Figure 7. The values of J are plotted against both ε_{yy} and ε^p_{yy} at x = 7.62 mm, the location of the extensometer.

The crack growth data were measured by Solomon at six different plastic strain levels, $\Delta\varepsilon_p$ = 0.001, 0.002, 0.005, 0.01, 0.02 and 0.05. The J-values at these six strain levels were calculated for the three crack lengths. At these eighteen combinations of $\Delta\varepsilon_p$ and a, both the crack growth rates and J-values are obtained. The results are shown in Figure 8.

For a strain-controlled fatigue test, the stabilized hysteresis loop is symmetrical, as shown in Figure 9. When the applied compression is high enough, a crack will close. The exact value of the stress or strain at which a crack will close is unknown. It will be assumed that during the lower half of the cycle when the applied stress is negative, a crack will close and lose its effectiveness as suggested by Haigh and Skelton [10]. Only the applied J corresponds to the positive part of the loading cycle (ABC in Figure 9) are used for crack growth data correlation.

In this part of the loading cycle, the relation between stress and strain follows the curve ABC. This segment of the stress-strain curve consists of the elastic and plastic parts. The plastic part is $\Delta\varepsilon_p$ and the plastic part is $\Delta\varepsilon_e/2$. The value of ΔJ for Solomon's specimen was evaluated at the plastic strain range $\Delta\varepsilon_p$ tested, and it corresponds to the ΔJ along the loading curve ABC in Figure 9.

The stress-strain relation along ABC differs slightly from the cyclic stress-strain curve. However, the cyclic stress-strain curve was used to calculate the crack tip field for Solomon's test. The values of J are strongly dependent on strain and much less on stress, therefore this approximation will introduce a rather small error. Furthermore, the stress-strain relation along ABC depends on the applied strain range. It varied from one specimen to another and it is unknown.

The correlation of da/dN with ΔJ for Solomon's test is shown in Figure 8. The correlation is better than with either $\Delta(PK)$ or ΔK_ε as shown in Figure 3. The data in Figure 8 give the empirical relation

$$\frac{da}{dN}\ (\text{mm/cycle}) = 0.7 \times \Delta J^{1.7} \qquad (11)$$

for Solomon's 1018 steel. ΔJ is in MPa-m. Equation (11) is also plotted in Figure 1 as the dashed line. The data for 1018 steel are within the data band of A533B steel. It is well known that fatigue crack growth data of low and medium carbon steels are all close together. However, in order to use the correlation for engineering applications, it is desirable to compare the measured and calculated ΔJ.

CONCLUSIONS

In general-yielding cyclic-loading, fatigue crack growth rate correlates very well with the calculated ΔJ values for specimens tested at six different cyclic strain ranges. In order to predict fatigue crack growth rates in engineering structures, it is necessary to establish the correlation between da/dN and calculated ΔJ.

REFERENCES

[1] Dowling, N.E. and Begley, J.A., "Fatigue Crack Growth During Gross Plasticity and the J-integral," Mechanics of Crack Growth, ASTM STP, Vol. 590, 1976, pp. 80-103.

[2] Dowling, N.E., "Crack Growth During Low-Cycle Fatigue of Smooth Axial Specimens," Cyclic Stress-Strain and Plastic Deformation Aspects of Fatigue Crack Growth, ASTM STP, Vol. 637, 1977, pp. 97-121.

[3] Shih, C.F. and Hutchinson, J.W., "Fully Plastic Solutions and Large Scale Yielding Estimations for Plane Stress Crack Problems," J. Engineering Materials and Technology, 1976, pp. 298-295.

[4] El Haddad, M.E. and Mukherjee, B., "Elastic-Plastic Fracture Mechanics Analysis of Fatigue Crack Growth," Elastic-Plastic Fracture: Second Symposium, Vol. II - Fracture Resistance Curves and Engineering Applications, ASTM STP Vol. 803, 1983, pp. II-689 - II-707.

[5] Tanaka, T. Hoshide, and Nakata, M., "Elastic-Plastic Crack Propagation Under High Cyclic Stresses," Elastic-Plastic Fracture: Second Symposium, Vol. II - Fracture Resistance Curves and Engineering Applications, ASTM STP Vol. 803, 1983, pp. II-708 - II-722.

[6] Kaisand, L.R. and Mowbray, "Relationships Between Low-Cycle Fatigue and Fatigue Crack Growth Rate Properties," Journal of Testing and Evaluation, JTEVA, Vol. 7, No. 5, Sept. 1979, pp. 270-280.

[7] Tomkins, B., "The Development of Fatigue Crack Propagation Models for Engineering Applications at Elevated Temperatures," Journal of Engineering Materials and Technology, Trans. of ASME, Series H., Vol. 97, 1975, pp. 289-297.

[8] Tomkins, B., Sumner, G., and Wareing, J., in Inter. Symposium on Low Cycle Fatigue Strength and Elasti-Plastic Behaviour of Materials, Deutscher Verband für Material Prüfung, Berlin, 1979, pp. 495-507.

[9] Solomon, H.D., "Low Cycle Fatigue Crack Propagation in 1018 Steel," J. of Materials, JMLSA, Vol. 7, No. 3, Sept. 1972, pp. 299-306.

[10] Haigh, J.R. and Skelton, R.P., "Fatigue Crack Growth Rates and Thresholds in Steels under Oxidising Conditions," Materials Science and Engineering, Vol. 36, 1978, pp. 17-25.

[11] Brown, M.W., Liu, H.W., Kfouri, A.P., and Miller, K.J., "An Analysis of Fatigue Crack Growth Under General Yielding Conditions," Advances in Fracture, edited by D. Francois et al., Pergamon Press, Oxford and New York, 1980.

[12] Zheng, Minzhong and Liu, H.W., "Crack Tip Field and Fatigue Crack Growth in General Yielding and Low Cycle Fatigue," NASA Contract Report 174686 to Lewis Research Center, Sept. 1984.

[13] Schijve, J. and Broek, D., "Crack-propagation-test based on a gust spectrum with variable amplitude loading," Aircraft Engineering, 34 (1962) pp. 314-316.

[14] Hutchinson, J.W., "Singular Behaviour at the End of a Tensile Crack in a Hardening Material and Plastic Stress and Strain Field at a Crack Tip," J. of Mech. and Phys. of Solids, Vol. 16, 13, 1968, p. 377.

[15] Rice, J.R. and Rosengren, G.F., "Plane Strain Deformation Near a Crack Tip in a Power-Law Hardening Material," J. of Mech. and Phys. of Solids, Vol. 16, 13, 1968, p. 1.

(16) McMeeking, R.M. and Parks, D.M., "On criterion for J dominance of crack tip fields in large scale yielding", ASTM STP 668, (1979) 175-194.

(17) Shih, C.F. and German, M.D., "Requirement for a one parameter characterization of crack tip field by the H.R.R. singularity", Int. J. of Fracture, 17, (1981), 27-43.

(18) Liu, H.W. and Zhuang, Tao, "A dual-parameter elastic-plastic fracture criterion", Accepted for publication in the Int. J. of Fracture, 1985

TABLE 1

COMPOSITION OF THE 1018 STEEL AND A533B PRESSURE VESSEL STEEL

	C	Mn	P	S	N	O	H	Ni	Mo	Si
1018 Steel	0.18	0.89	0.013	0.022	0.0047	0.0019	<0.002	0	0	0
A533B Steel	0.25	1.15∿1.50	0.034	0.40	0	0	0	0.4∿0.7	0.45∿0.60	0.15∿0.30

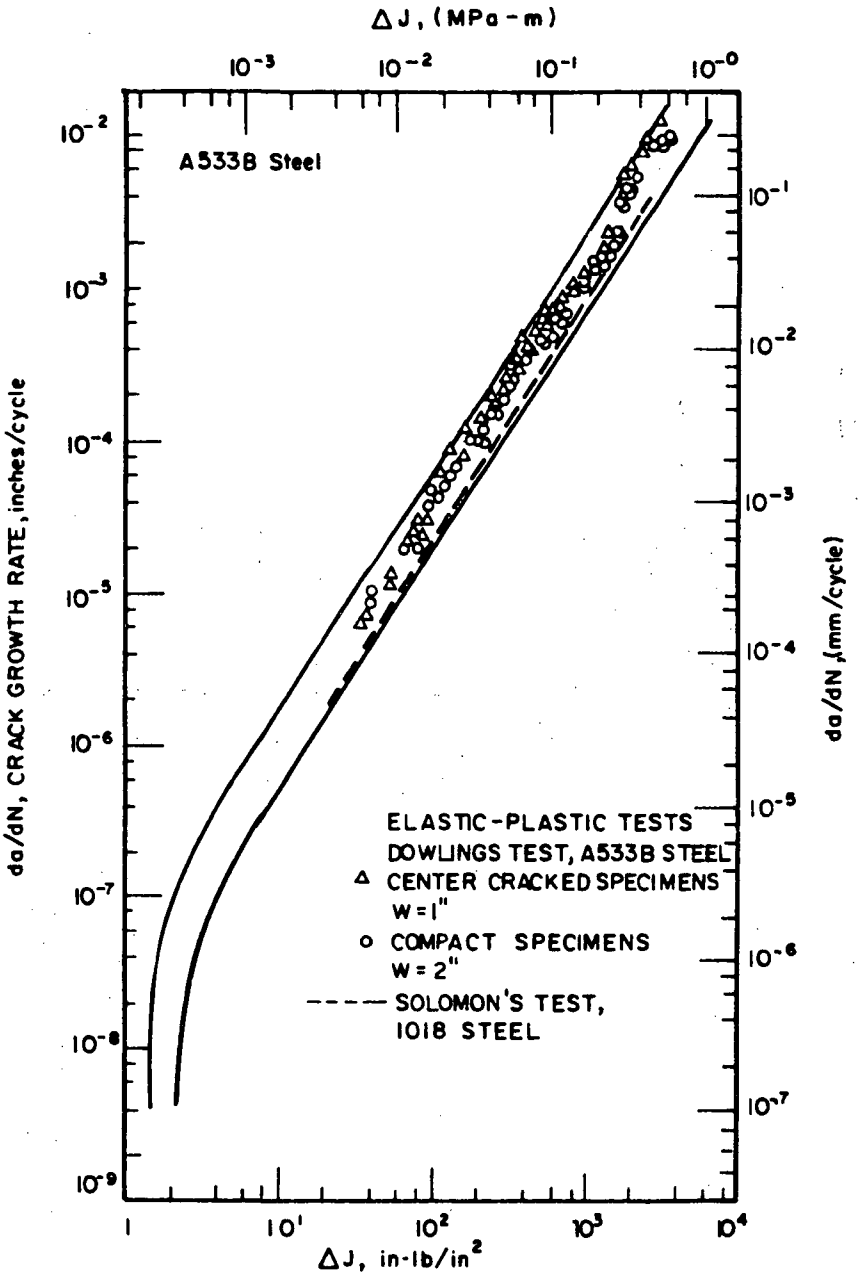

Figure 1. Fatigue crack growth rate versus ΔJ [1].

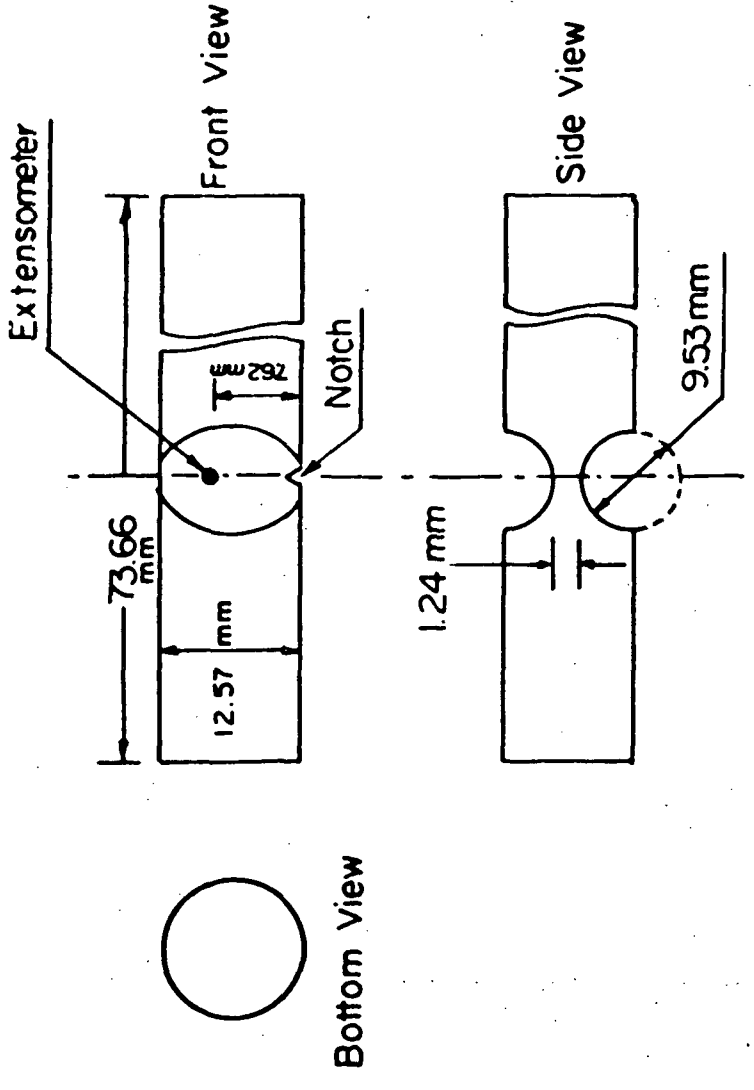

Figure 2a. Dimensions of Solomon's specimen [9].

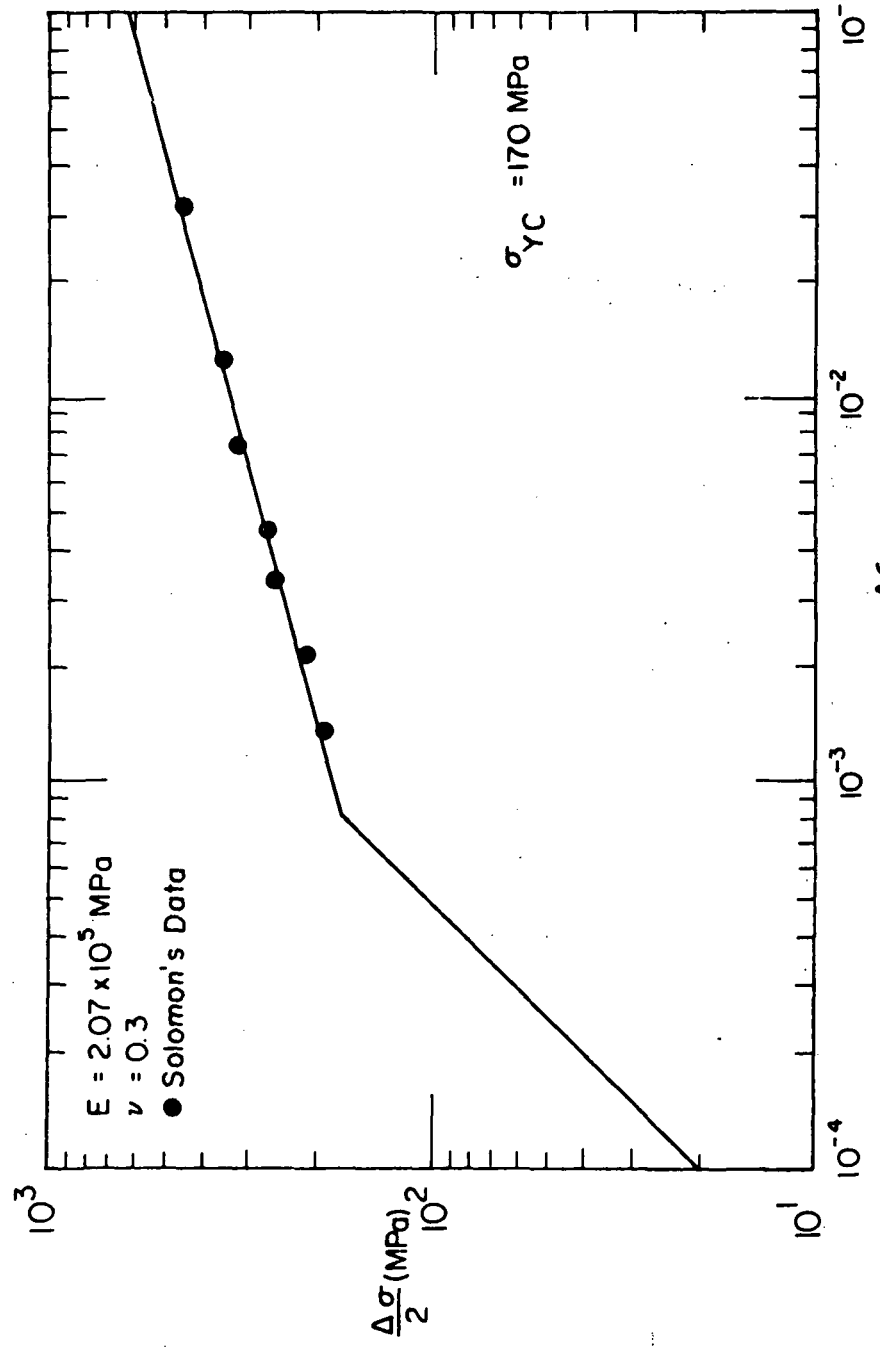

Figure 2b. Cyclic stress-strain curve, 1018 steel [9].

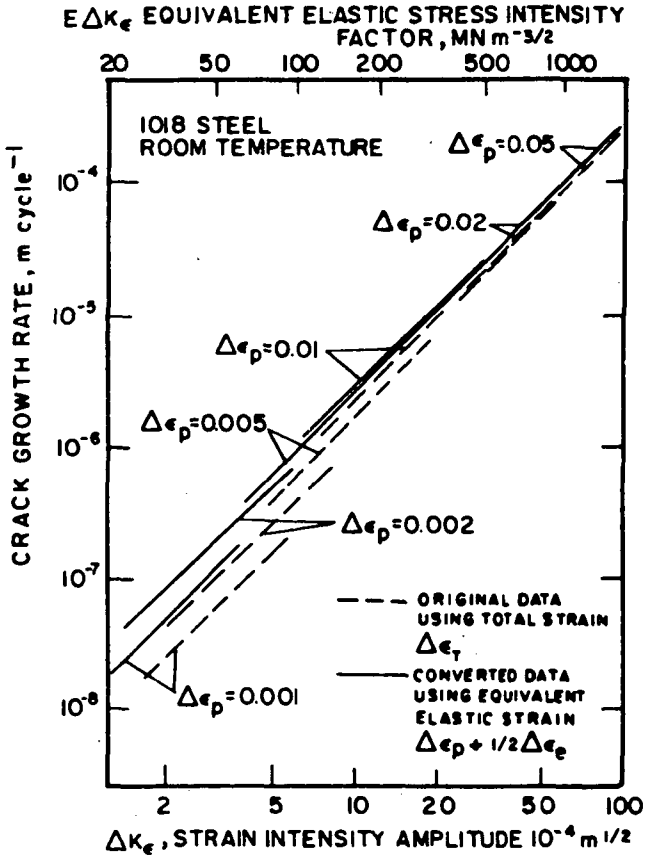

Figure 3. Comparison of equations (7) and (8) using Solomon's data [10].

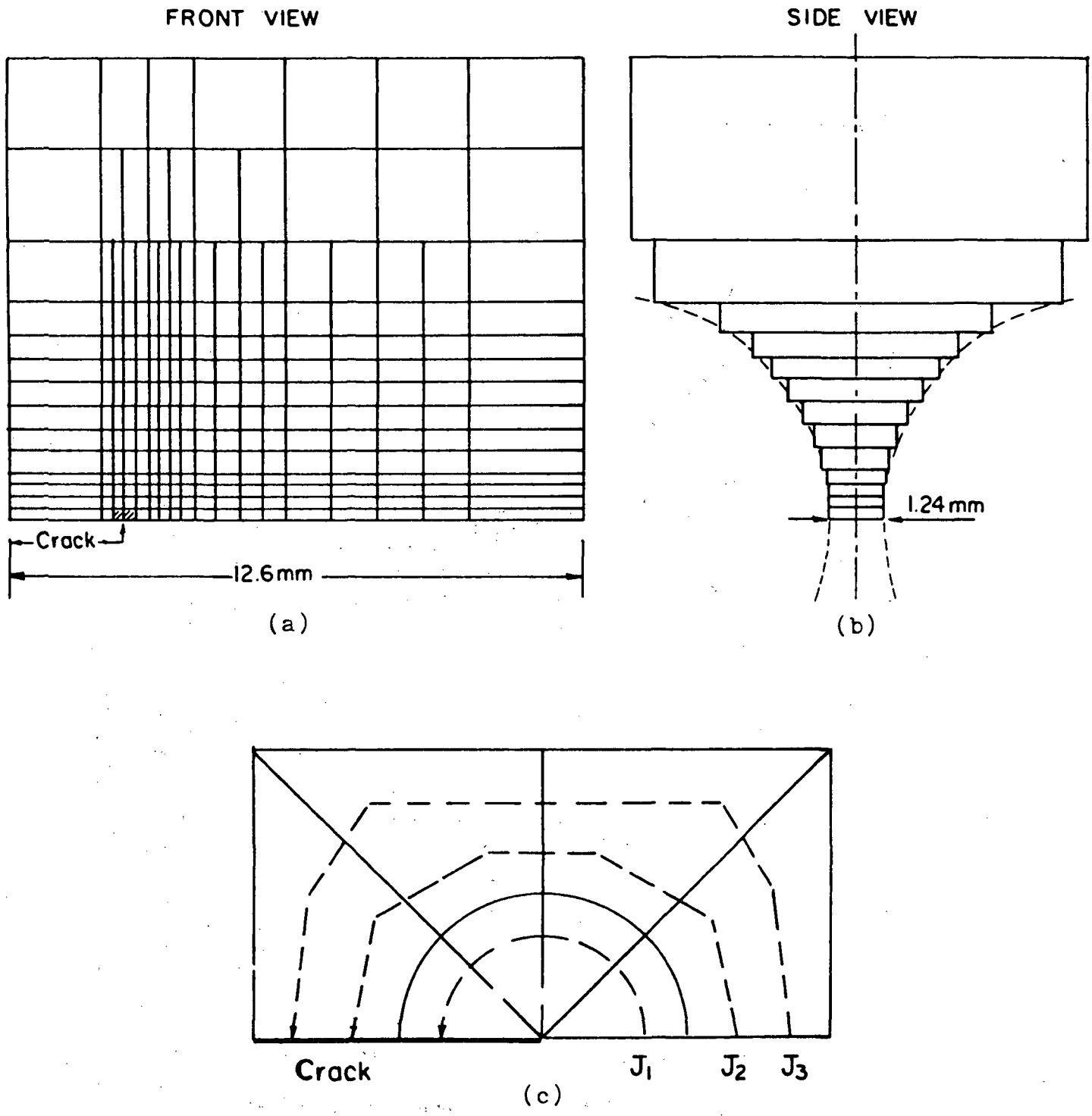

Figure 4. Finite element idealization for Solomon's specimen, showing (a) top half of the specimen, (b) cross section, and (c) crack tip elements.

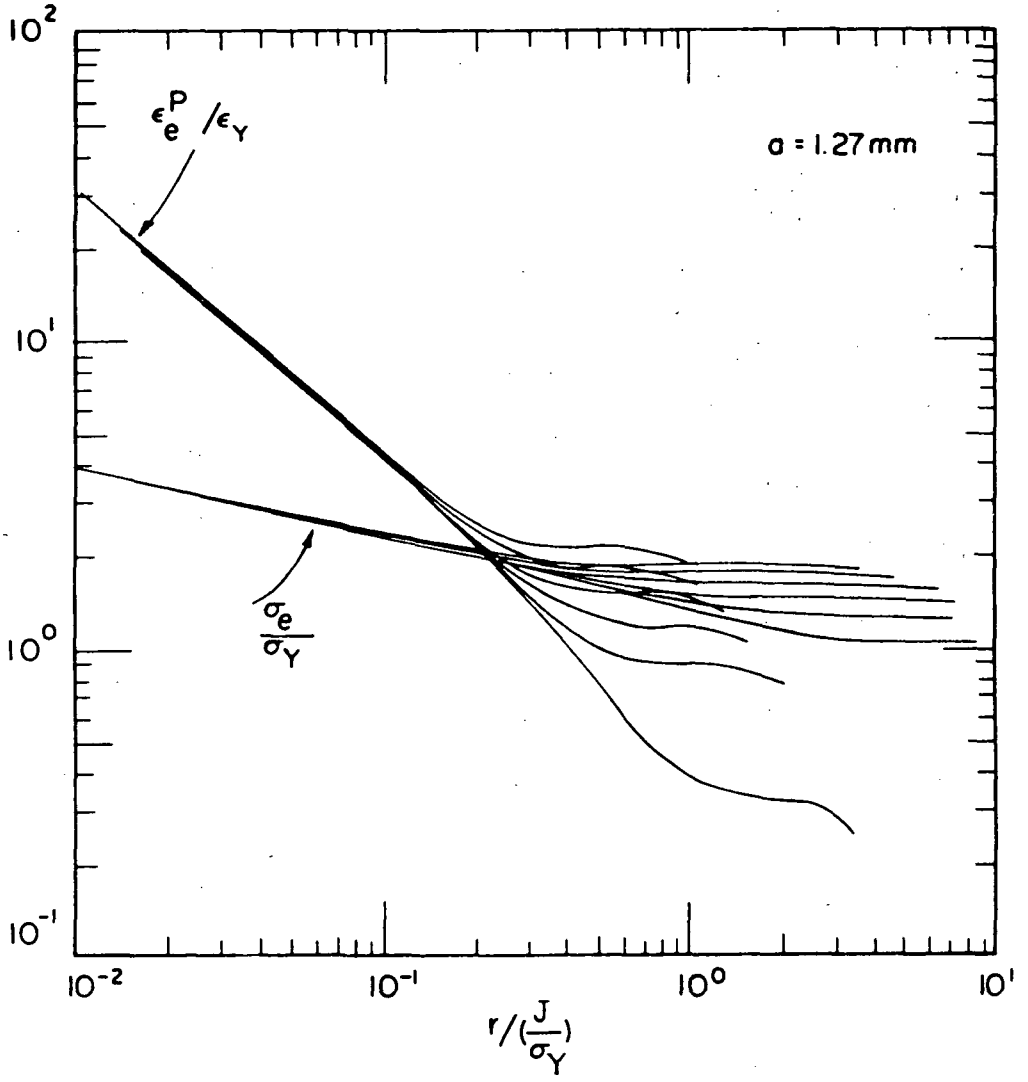

Figure 5a. Normalized effective plastic strain (ε_e^p) and effective stress (σ_e) distributions ahead of the crack tip for Solomon's specimen.

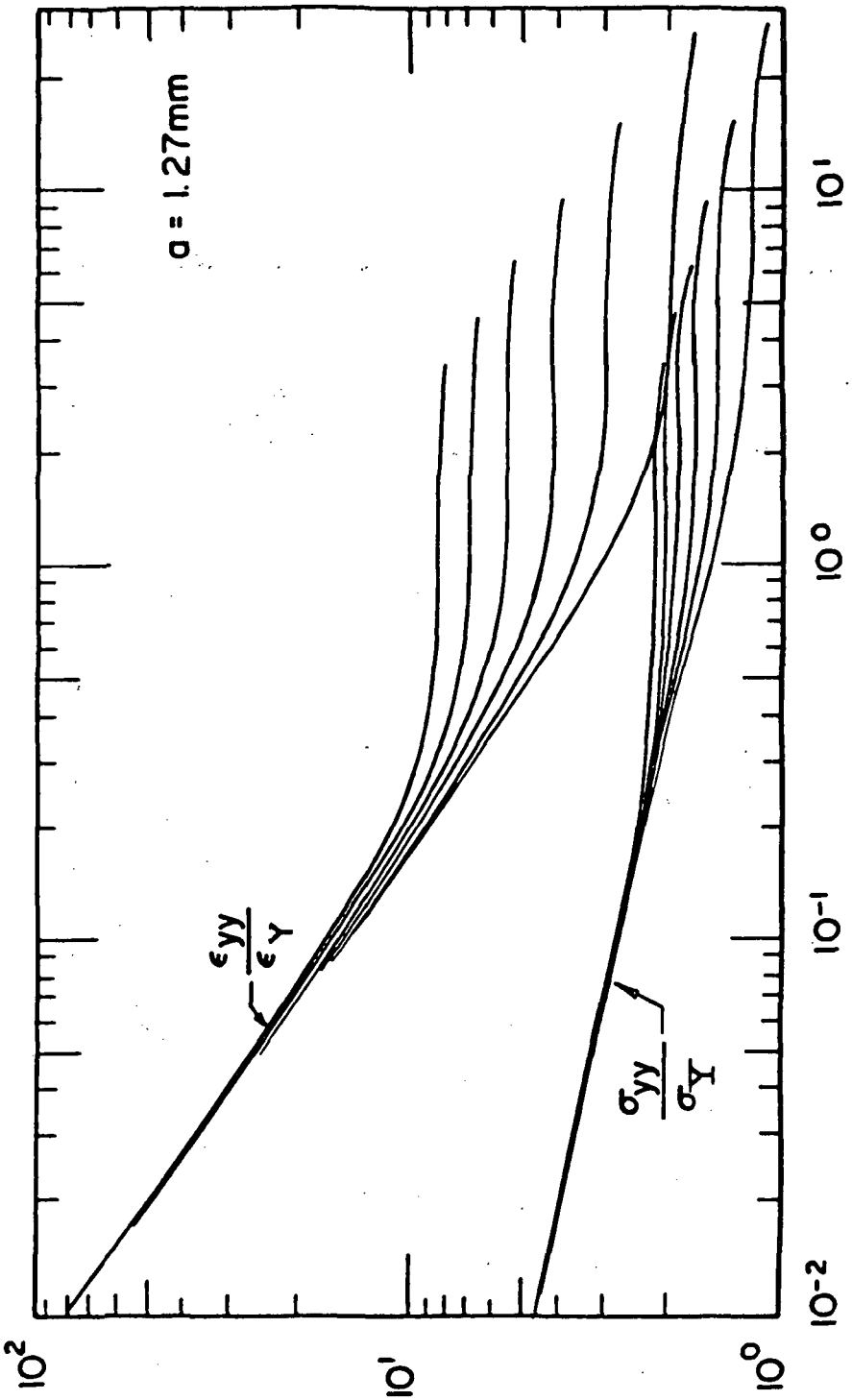

Figure 5b. Normalized strain (ϵ_{yy}) and stress (σ_{yy}) distributions ahead of the crack tip for Solomon's specimen.

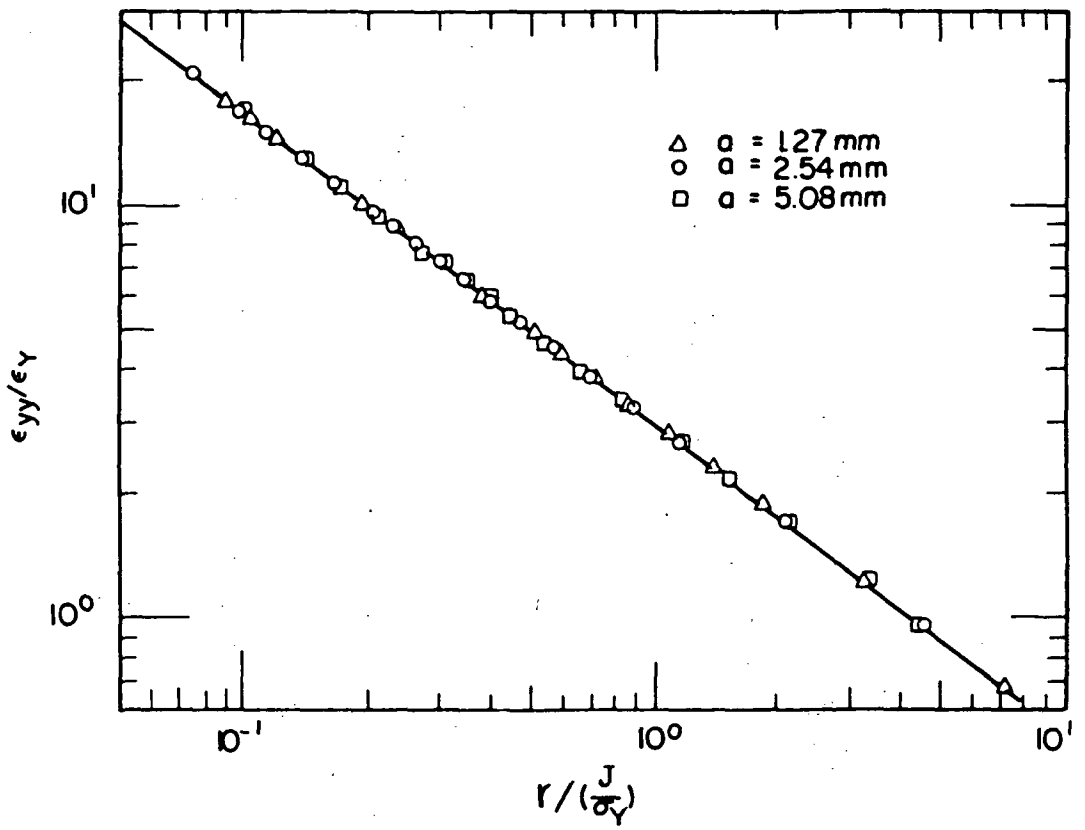

Figure 6. Normalized strain (ε_{yy}) distribution near the crack tip for three different crack lengths.

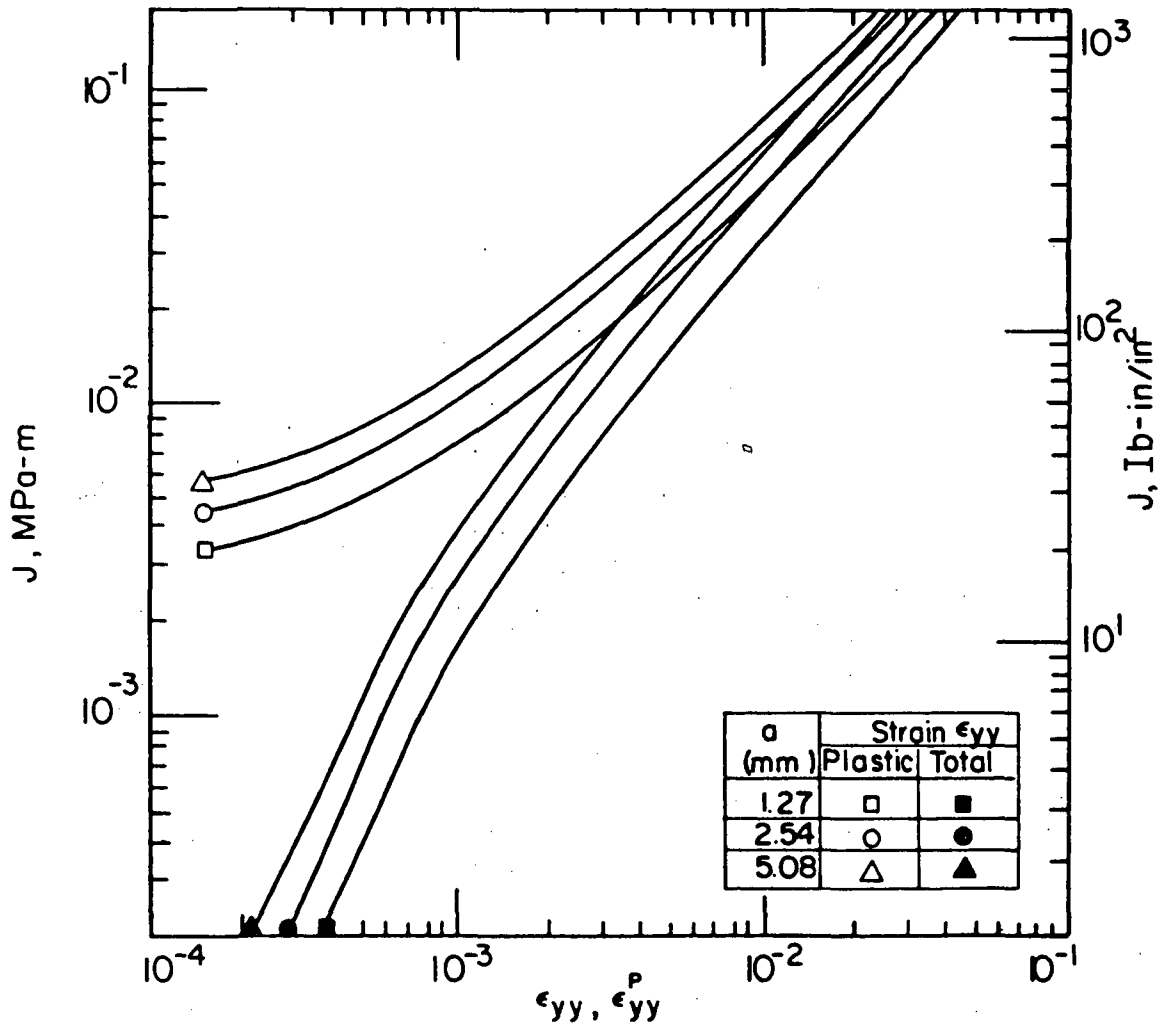

Figure 7. J-integral dependence on applied strains at x = 7.62 mm, the location of the monitoring extensometer.

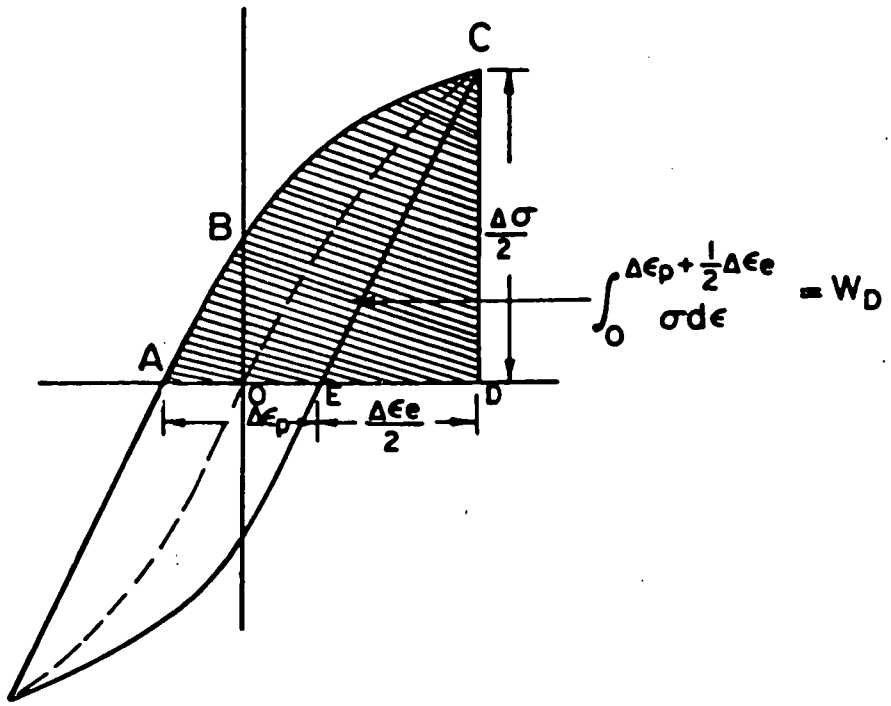

Figure 8. Cyclic stress-strain loop and the deformation work density, W_D.

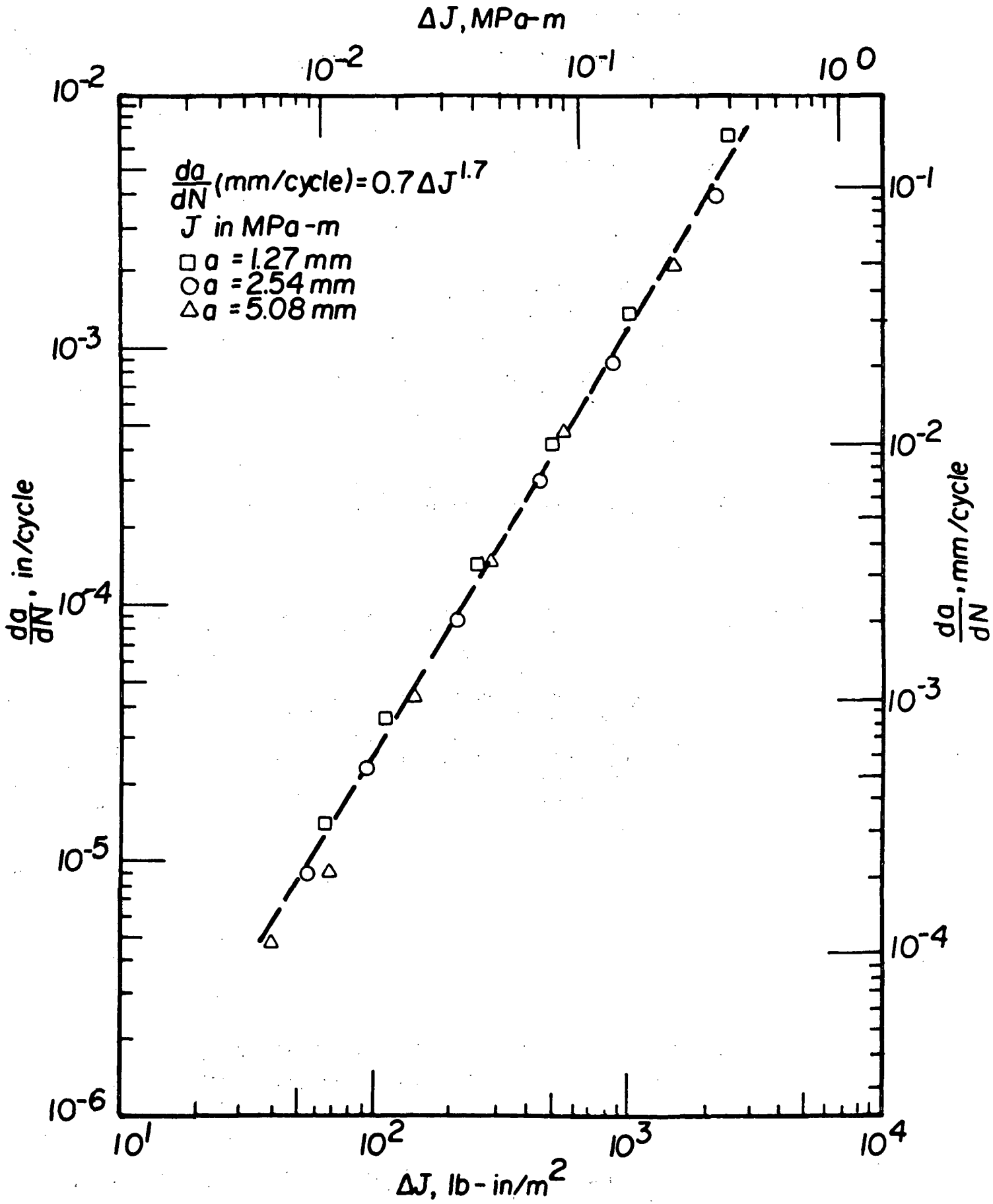

Figure 9. Correlation of da/dN versus ΔJ for Solomon's tests.

1. Report No.	2. Government Accession No.	3. Recipient's Catalog No.
NASA CR-175049		

4. Title and Subtitle	5. Report Date
Fatigue Crack Growth Under General-Yielding Cyclic-Loading	February 1986
	6. Performing Organization Code
7. Author(s)	8. Performing Organization Report No.
Zheng Minzhong and H.W. Liu	None
	10. Work Unit No.
9. Performing Organization Name and Address	11. Contract or Grant No.
Sycrause University Dept. of Mechanical and Aerospace Engineering Syracuse, New York 13210	NAG 3-348
	13. Type of Report and Period Covered
12. Sponsoring Agency Name and Address	Contractor Report
National Aeronautics and Space Administration Washington, D.C. 20546	14. Sponsoring Agency Code
	533-04-12

15. Supplementary Notes

Project Manager, Jack Telesman, Structures Division, NASA Lewis Research Center, Cleveland, Ohio 44135. This research was sponsored by the HOST Program.

16. Abstract

In low cycle fatigue, cracks are initiated and propagated under general-yielding cyclic-loading. For general-yielding cyclic-loading, Dowling and Begley have shown that fatigue crack growth rate correlates well with the measured ΔJ. The correlation of da/dN with ΔJ has also been studied by a number of other investigators. However, none of these studies has correlated da/dN with ΔJ calculated specifically for the test specimens. Solomon measured fatigue crack growth in specimens in general-yielding cyclic-loading. The crack tip fields for Solomon's specimens are calculated using the finite element method and the J-values of Solomon's tests are evaluated. The measured crack growth rate in Solomon's specimens correlates very well with the calculated ΔJ.

17. Key Words (Suggested by Author(s))	18. Distribution Statement
Fatigue crack growth; Elasto-plastic; J-integral	Unclassified - unlimited STAR Category 39

19. Security Classif. (of this report)	20. Security Classif. (of this page)	21. No. of pages	22. Price*
Unclassified	Unclassified	26	A03

*For sale by the National Technical Information Service, Springfield, Virginia 22161

National Aeronautics and
Space Administration

Lewis Research Center
Cleveland, Ohio 44135

SECOND CLASS MAIL

ADDRESS CORRECTION REQUESTED

Official Business
Penalty for Private Use $300

Postage and Fees Paid
National Aeronautics and
Space Administration
NASA-451